PERGAMON

Journal of Geodynamics 35 (2003) 259–272

JOURNAL OF
GEODYNAMICS

www.elsevier.com/locate/jog

Geodetic measurements of crustal deformation on NW–SE faults of the Betic Cordillera, southern Spain, 1999–2001

A.M. Ruiz[a,*], G. Ferhat[b], P. Alfaro[c], C. Sanz de Galdeano[d], M.C. de Lacy[e], G. Rodríguez-Caderot[f], A.J. Gil[a]

[a]*Departamento de Ingeniería Cartográfica, Geodésica y Fotogrametría, Escuela Politécnica Superior de Jaén, Universidad de Jaén, C/. Virgen de la Cabeza, 2, 23071 Jaén, Spain*
[b]*ENSAIS- UMR MAP CNRS/MCC 694, 24 Boulevard de la Victoire, 67084 Strasbourg, France*
[c]*Departamento de Ciencias de la Tierra y Medio Ambiente, Universidad de Alicante, Apdo. 99, San Vicente del Raspeig, Alicante, Spain*
[d]*Instituto Andaluz de Ciencias de la Tierra, C.S.I.C., Universidad de Granada, 18071 Granada, Spain*
[e]*Facolta di Ingegneria di Como. Instituto Politecnico di Milano, Piazza Le Gerbetto, 22100 Como, Italy*
[f]*Departamento de Astronomía y Geodesia, Facultad de Ciencias Matemáticas, Universidad Complutense de Madrid, Madrid, Spain*

Accepted 13 May 2002

Abstract

The Granada basin, located in the central sector of the Betic Cordillera, is one of the most seismically active zones of the Iberian Peninsula. For the first time, a geodetic network along the Padul fault and two levelling profiles (Genil and Viznar) crossing the Granada fault were operated to detect crust micro-deformations in this area. Three years of terrestrial geodetic measurements are analysed to characterize the behaviour of these faults in a low to moderate strain rate environment. After the comparison of these three campaigns, we can conclude that there is no significant short-term movement of the Padul fault. Granada fault measurements show significant differences between 1999 and 2001 campaigns in Viznar profile. However, more data are needed to correlate this displacement to the tectonic activity.

1. Introduction

Near-field geodetic surveying have been frequently used to detect interseismic and coseismic deformation. In most cases, these studies have been operated across active and potentially active faults with high or very high activity rates. In this paper we have selected two faults located in a low to moderate strain-rate environment, the Granada basin.

* Corresponding author. Fax: + 34-953-012-343.
E-mail address: amruiz@ujaen.es (A.M. Ruiz).

0264-3707/03/$ - see front matter
PII: S0264-3707(02)00134-5

This basin is located inside a wide collision zone between African and Eurasian plates, which converge approximately at 5 mm/a according to Argus et al. (1989) and the NUVEL-1A plate motion model (DeMets et al., 1994).

The study area, located in the central sector of the Betic Cordillera, is an area with one of the highest rates of microseismic activity of the Iberian Peninsula, with mb$\leqslant$5.5 earthquakes (De Miguel et al., 1989). Occasionally, these earthquakes are grouped in seismic series, as the last which occurred in the city of Granada between 4 and 12 July 1998. During those nine days, 29 earthquakes with magnitude less than 2.0, 11 earthquakes with magnitude between 2.0 and 3.0, and 5 earthquakes with magnitude higher than 3.0 occurred. The two most important recent earthquakes that occurred in this oriental sector of the Granada basin are the 1956 Albolote earthquake with magnitude 5.0, and the 1911 Santa Fe earthquake with magnitude 4.9. There is evidence of several historic earthquakes as well. For example the 1806 Santa Fe earthquake which reached M.S.K. intensity IX, or the 1526 and 1431 Granada earthquakes which reached M.S.K. intensity VIII and IX respectively. Also, paleoseismic studies show that during the Late Pleistocene and the Holocene, the region has experienced several moderate-high magnitude earthquakes (Alfaro et al., 2001).

The seismotectonic studies done in the central sector of this Alpine orogen, based on the focal mechanism, reveal that nowadays, the region is subject to a NW–SE compressive stress field with a NE–SW linked extension (Galindo-Zaldívar et al., 1999; Herraiz et al., 2000).

The NE–SW extension is accommodated by normal faults in various orientations, amongst which the NW–SE faults stand out (Fig. 1). These normal faults show geological evidence of recent activity (fault scarps, triangular facets, deformed alluvial fans, etc.) (Lhénaff, 1965; Estévez and Sanz de Galdeano, 1983; Riley and Moore, 1993; Calvache et al., 1997; Sanz de Galdeano and López Garrido, 1999). From the different heights of Neogene and Quaternary materials displaced by these faults, Sanz de Galdeano (1996) and Keller et al. (1996) have estimated an average rate of uplift for the Sierra Nevada western sector from 0.4 to 0.6 mm/a, and occasionally of 0.8 mm/a.

In order to quantify the present deformation of these NW–SE normal faults and to compare this with geological estimations, a geodetic control has been established. In this study two major faults have been selected; the Padul fault, owing to widespread geomorphological evidence of recent activity in the area, and the Granada fault, which crosses the city of Granada, selected because it is a poorly studied normal fault located in a highly population urban area. In this paper, the recent tectonic activity and the associated seismicity of these two faults are analysed, the geodetic activities developed are described, and finally, the results of the first three campaigns are presented.

2. Active faults

2.1. The Padul fault

The Padul normal fault offsets the metamorphic Triassic carbonates of the Betic Cordillera Internal Zone (Alpujarride Complex) (Fig. 2). This NW–SE fault (locally E–W) is approximately 15 km long and has various segments which dip towards the SW and S.

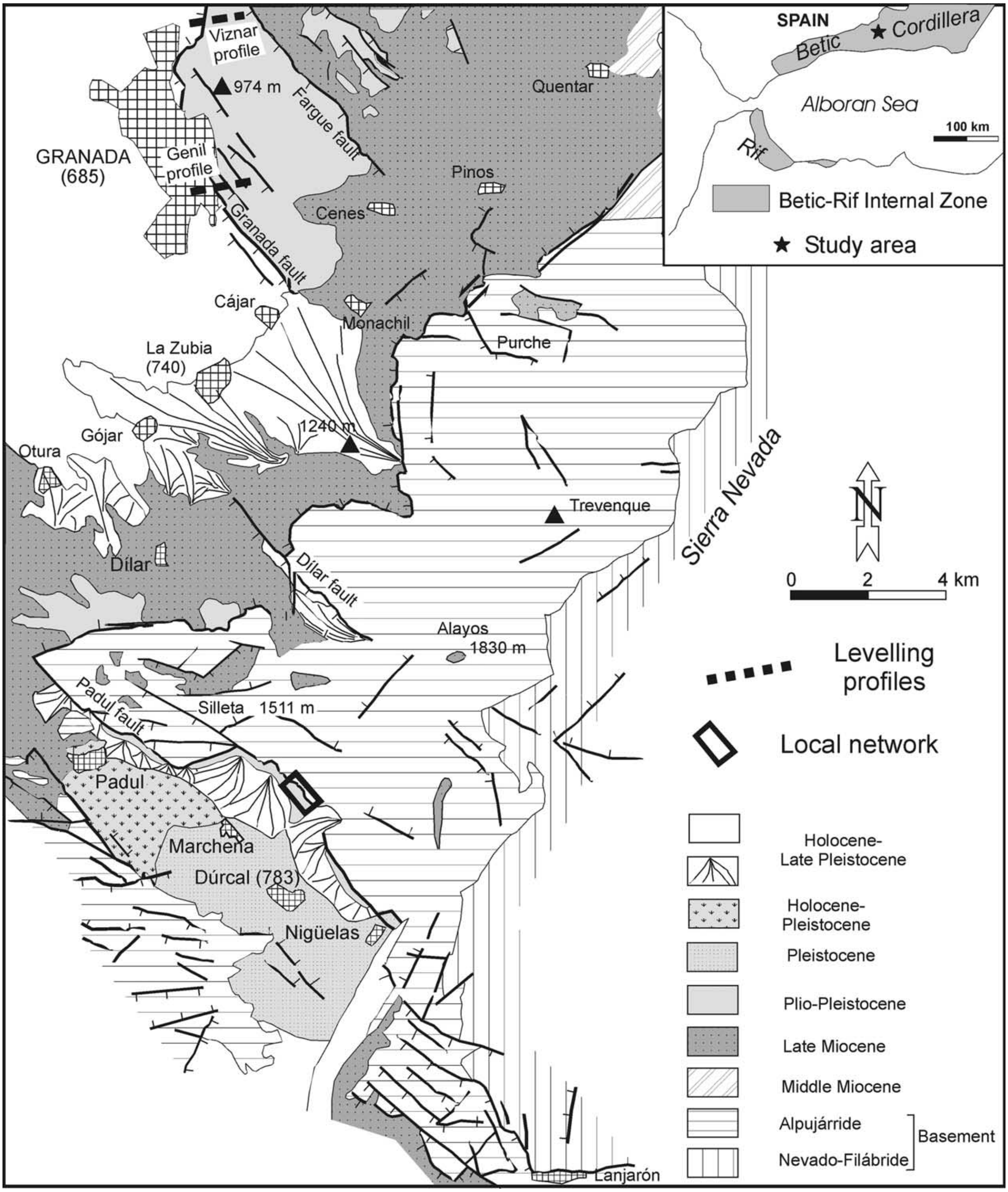

Fig. 1. Simplified geological map of the study area with location of the levelling profiles at the Granada fault and the local network at the Padul fault.

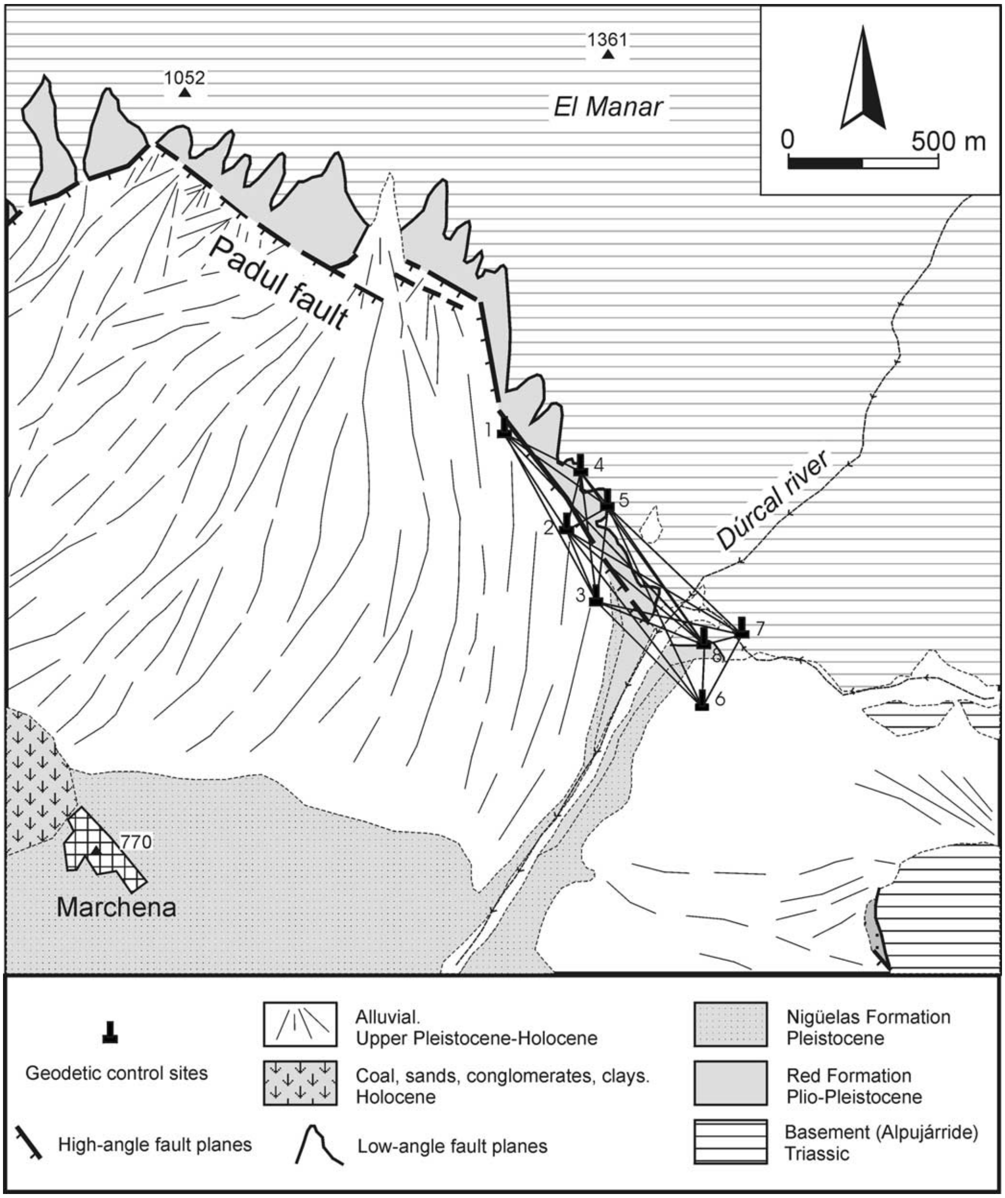

Fig. 2. Padul fault segment in which the eight sites of the local network are located.

The footwall is constituted of Alpujarride basement and the fault hanging wall is comprised of Quaternary and Plio-Quaternary sediments deposited above the Alpujarride basement and upper Miocene rocks (Fig. 3). Santanach et al. (1980) estimate that the vertical throw of this fault is approximately 800 m.

There is both geomorphological and tectonic evidence to indicate that this fault continues to be active at present (fault scarps, deformed Holocene alluvial fans, triangular facets, strong down-cutting in the drainage network, Holocene peat deposits dipping against the fault plane, etc)

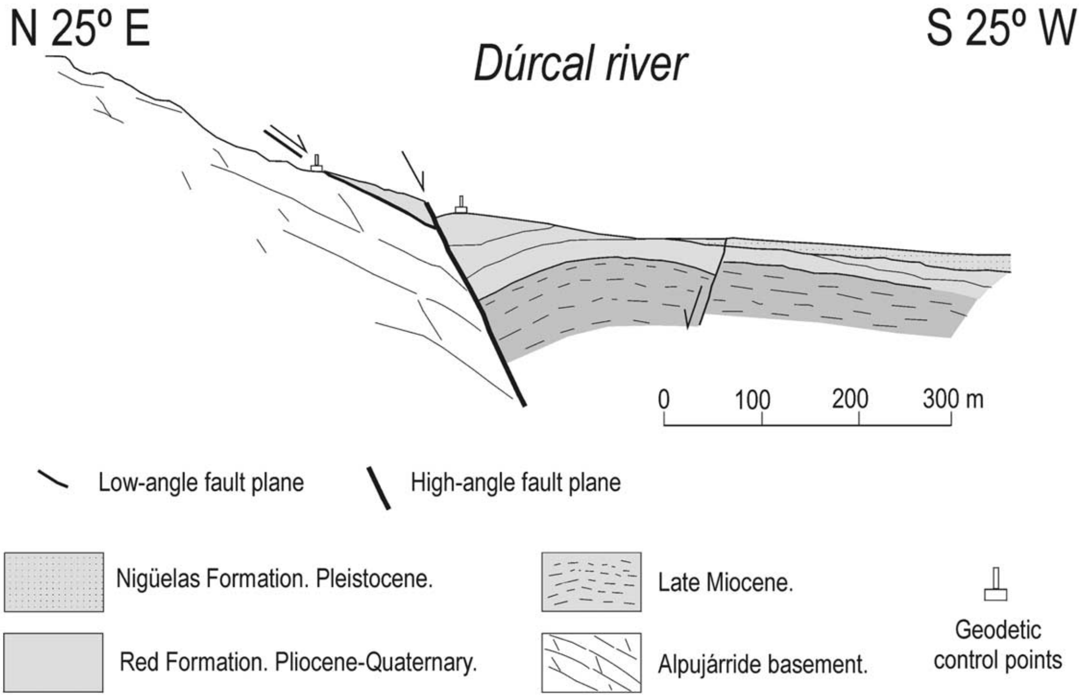

Fig. 3. Geologic cross-section of the Padul fault along the Dúrcal river showing a general location of geodetic control sites.

(Lhénaff, 1965; Riley and Moore, 1993; Calvache et al., 1997). From the different elevations of the Red Formation Plio-Pleistocene deposits displaced by the *Padul* fault, Sanz de Galdeano et al. (in press) deduce an average rate of uplift of 0.35 mm/a over the last million years.

Analysis of the slickensides (striations, corrugations,...) present on the fault planes show that the principal displacement has a marked left-lateral horizontal component.

The level of seismic activity along the Padul fault is very low. No evidence of moderate or high magnitude historic earthquakes exists. In the period 1980–1996 only one earthquake of magnitude higher than 3.5 has occurred. In spite of this low recent seismic activity, there is geological evidence of moderate to high-magnitude earthquakes during the Quaternary (Alfaro et al., 2001).

2.2. The Granada fault

This NW–SE fault runs between the northern part of the town of Pulianas and the south of the town of Monachil (Fig. 4). Its central part, which crosses the city of Granada, has a N–S segment. Although it does not have a clear fault plane along its trace, various prominent fault scarps, some tens of metres high, exist which show the recent activity of this fault.

The Alhambra Formation rocks outcrop in the footwall of the Granada fault. This formation is composed of alluvial fan deposits of Late Pliocene-Pleistocene age. Probably its age is less than 1 million years (Keller et al., 1996; Aguirre, 1957; Ruiz-Bustos, 1972; Ruiz-Bustos et al., 1990). Detritic sediments of Late Pleistocene and Holocene age outcrop in the hanging wall.

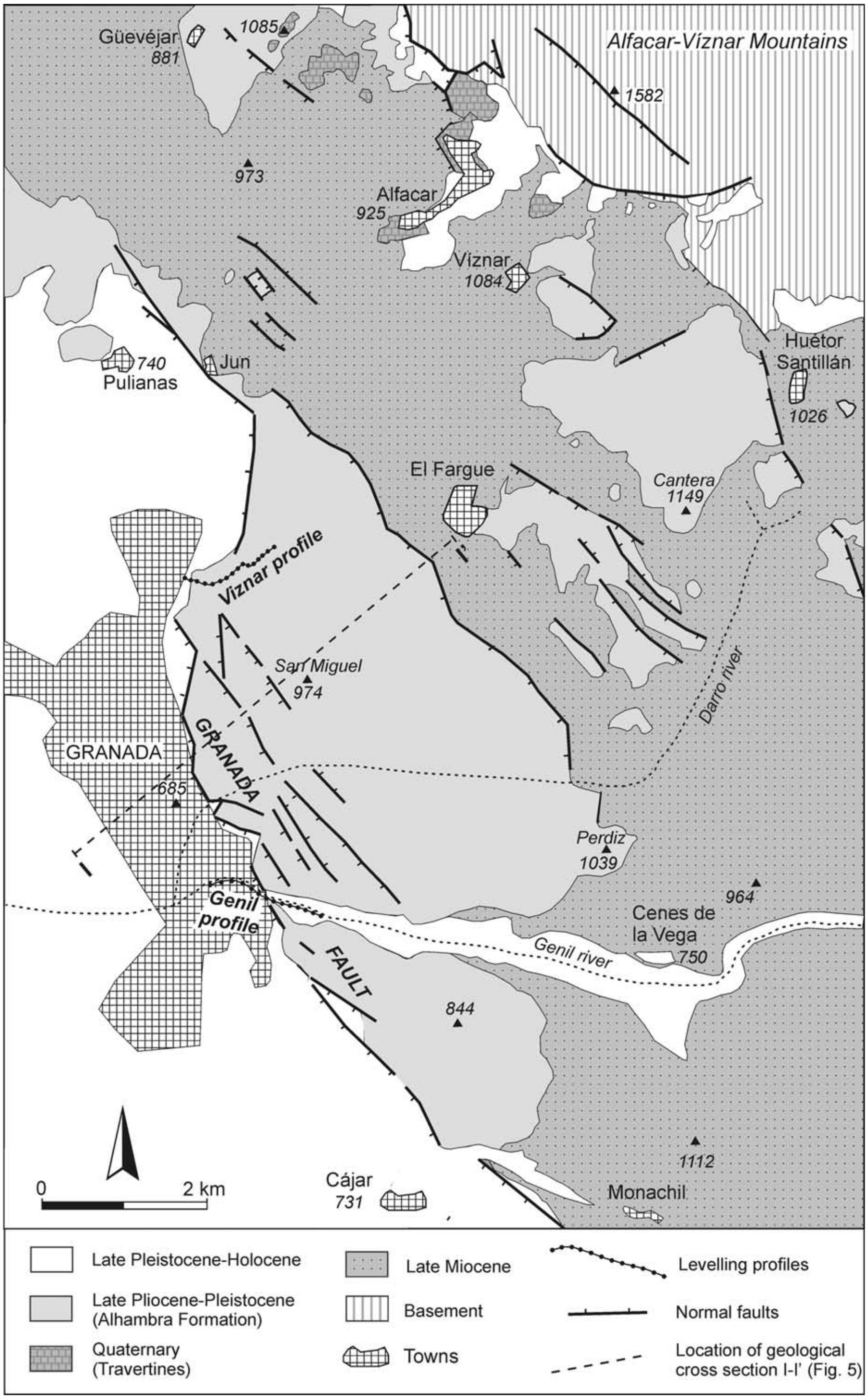

Fig. 4. Geologic map of the Granada surrounding area with location of the Granada fault, and the Viznar and Genil levelling profiles.

Keller et al. (1996) carried out a morphotectonic study near Granada. These authors analysed the normal faults that offset the Alhambra Formation rocks and calculated that the total vertical throw accumulated by these faults was about 600 m. In Fig. 5 it is possible to recognize 410 m of accumulated throw of the faults nearest to the city of Granada (Keller et al., 1996). Sanz de Galdeano et al. (in press) calculate that the vertical slip-rate of this fault is 0.38 mm/a over the last 0.8 million years.

There is prominent microseismic activity along its trace and in the nearby zones, but there is no evidence of the occurrence of large earthquakes associated with this fault. Although the epicentres of the recent seismic series of June 1998 are located along the trace of the Granada fault according to the dip of this fault (to the SW) and the depth of the earthquakes, they might be associated with another fault located several kilometres to the NE (probably the Fargue fault) (Sanz de Galdeano et al., in press).

3. Data and method

We analyze two kinds of geodetic data. Firstly, horizontal angles, vertical angles and distance measurements performed at the Padul fault; and secondly, measurements taken at the Granada fault. In December 1998, an eight-station Triangulation-Trilateration network was established along the Padul fault (Fig. 2) (Ruiz et al., 1999), and surveyed for the first time in February 1999, then in February 2000 and February 2001 by the Microgeodesy Research Group of the Jaén University (Spain) as part of a project to monitor ground deformations (Gil et al., 1999). This network is made up of eight reinforced concrete built pillars anchored to the rock and with a special centred device for geodetic instruments (Gil et al., 2000).

Eighty horizontal angles among sites were measured with the Wild T3000 electronic theodolite and the TCA2003 total station applying the Schreiber method (Bomford, 1980) in three different campaigns, February 1999, February 2000 and February 2001. Each angle between two sites was measured with two sets, that is, two pairs in each position of the graduated circle. In addition,

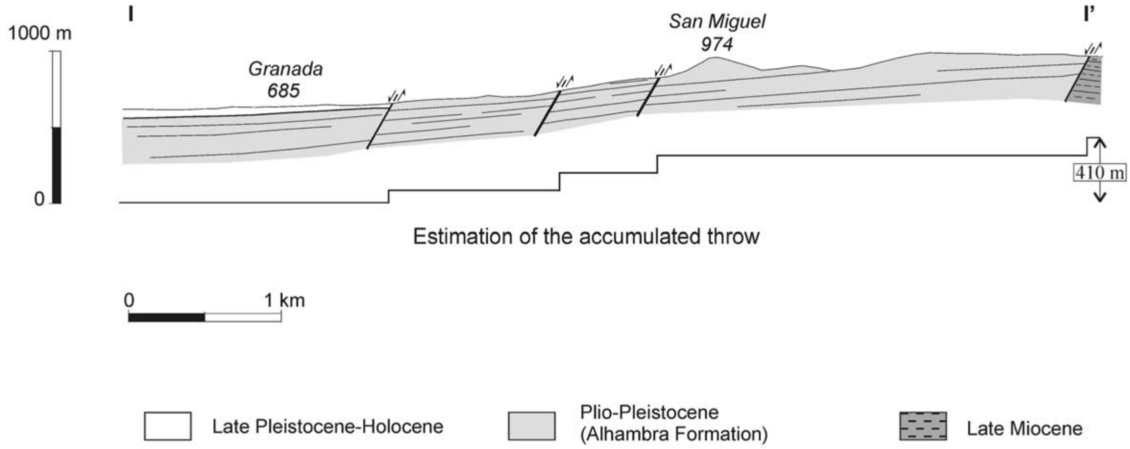

Fig. 5. Generalized geologic cross-section near Granada, illustrating vertical fault displacement produced by the activity of the Granada fault and others NW-SE normal faults (after Keller et al., 1996). Location is shown in Fig. 4.

each vertical angle measurement was taken four times. The standard deviation of a horizontal direction is 0.6–0.9 s of arc or about 2.9–4.3 microradians. The distances were observed by electronic distance measurement (EDM) using the infrared Distomat Wild DI3000 and the Leica TCA2003 instruments together with meteorological data measurements equipment at the endpoints. The forty spatial distances were calculated with a series of forty measurements each. The error model in the trilateration measurements can be predicted by a standard deviation (Savage and Prescott, 1973; Laurila, 1983)

$$\sigma = \sqrt{a^2 + (b \cdot D)^2} \tag{1}$$

where D denotes the measured distance expressed in kilometers, and a and b are constants. The values of a and b are 3 mm and 1 ppm for DI3000, and 1 mm and 1 ppm for TCA2003. Table 1 shows some statistics about the data.

To estimate the strain rates, we used a forward modelling network deformation analysis software package (Dong, 1993; Dong et al., 1998). Heights estimated by trigonometric levelling were corrected for geoid undulations in order to reduce spatial distances to International ellipsoid. DGPS with System 300 and System 500 Leica dual-frecuency receivers were used to obtain the approximate geodetic coordinates for the stations. For each station, we can estimate as many as four parameters: the two horizontal components of both the position and velocity vectors in a so-called 'free network' solution (Ferhat et al., 1998). The deformation parameters obtained are defined by Prescott et al. (1979). The angular shear strain rates ($\dot{\gamma}_1$ and $\dot{\gamma}_2$), and the maximum (total) shear strain rate ($\dot{\gamma}$) are respectively

$$\dot{\gamma}_1 = \dot{E}_{\mathrm{ee}} - \dot{E}_{\mathrm{nn}} \tag{2}$$

$$\dot{\gamma}_2 = 2\dot{E}_{\mathrm{en}} \tag{3}$$

$$\dot{\gamma} = \sqrt{\dot{\gamma}_1^2 + \dot{\gamma}_2^2} \tag{4}$$

where $\dot{E}_{\mathrm{nn}}$, $\dot{E}_{\mathrm{ee}}$ and $\dot{E}_{\mathrm{en}}$ are the strain rate tensor components in the north (n) and east (e) directions and the off-diagonal component respectively. A geometrical interpretation of those $\dot{\gamma}_1$ and $\dot{\gamma}_2$ can be found in Feigl et al. (1990). The shear rate parameter $\dot{\gamma}_2$ measures the decrease in the right angle between a ray pointing north and one pointing east. This decrease can be attributed to either right-lateral shear across a vertical fault striking east or to left-lateral shear across a fault striking north. Similarly, $\dot{\gamma}_1$ measures the decrease in the right angle between rays pointing northwest and northeast, due to right-lateral shear on a fault striking N45°W or left-lateral shear

Table 1
Some statistics about the data used in the 1999–2000–2001 inversion of the local geodetic network at Padul fault

Data	Horizontal directions		Vertical angles		Spatial distances	
	Values	rms (arcsecond)	Values	rms (arcsecond)	Values	rms (mm)
1999	112	0.73	40	1.13	40	10
2000	112	0.64	40	0.96	40	3
2001	112	0.58	40	0.93	40	3

on a fault striking N45°E. We also obtained the azimuth $\theta = \psi - 45^\circ$ to provide the orientation of the axis of the most compressive principal strain rate

$$\theta = \frac{1}{2} atan(-\dot{\gamma}_2/\dot{\gamma}_1) \text{ if } \dot{\gamma}_1 > 0 \tag{5}$$

$$\theta = \frac{1}{2} atan(-\dot{\gamma}_2/\dot{\gamma}_1) - \pi/2 \text{ if } \dot{\gamma}_1 < 0 \text{ and } \dot{\gamma}_2 > 0 \tag{6}$$

$$\theta = \frac{1}{2} atan(-\dot{\gamma}_2/\dot{\gamma}_1) + \pi/2 \text{ if } \dot{\gamma}_1 < 0 \text{ and } \dot{\gamma}_2 < 0 \tag{7}$$

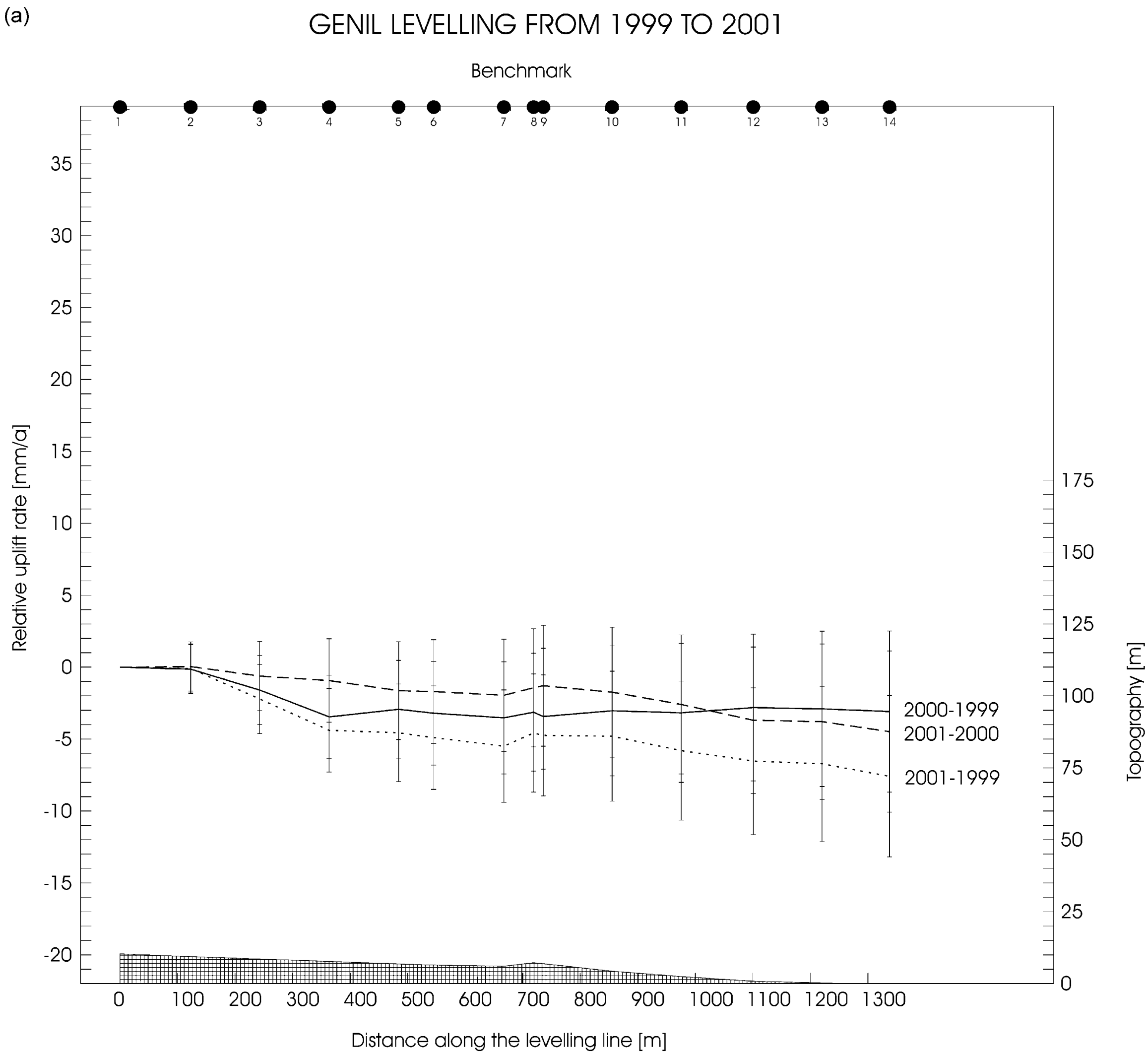

Fig. 6. Comparison of results between 2000–1999, 2001–1999 and 2001–2000 levelling campains in (a) Genil profile, and (b) Viznar profile. The topography is shown as the darker shaded profile on the bottom. An arbitrary vertical reference system has been adopted for benchmark heights. Thin vertical bars are 3.29 σ cumulative error bounds.

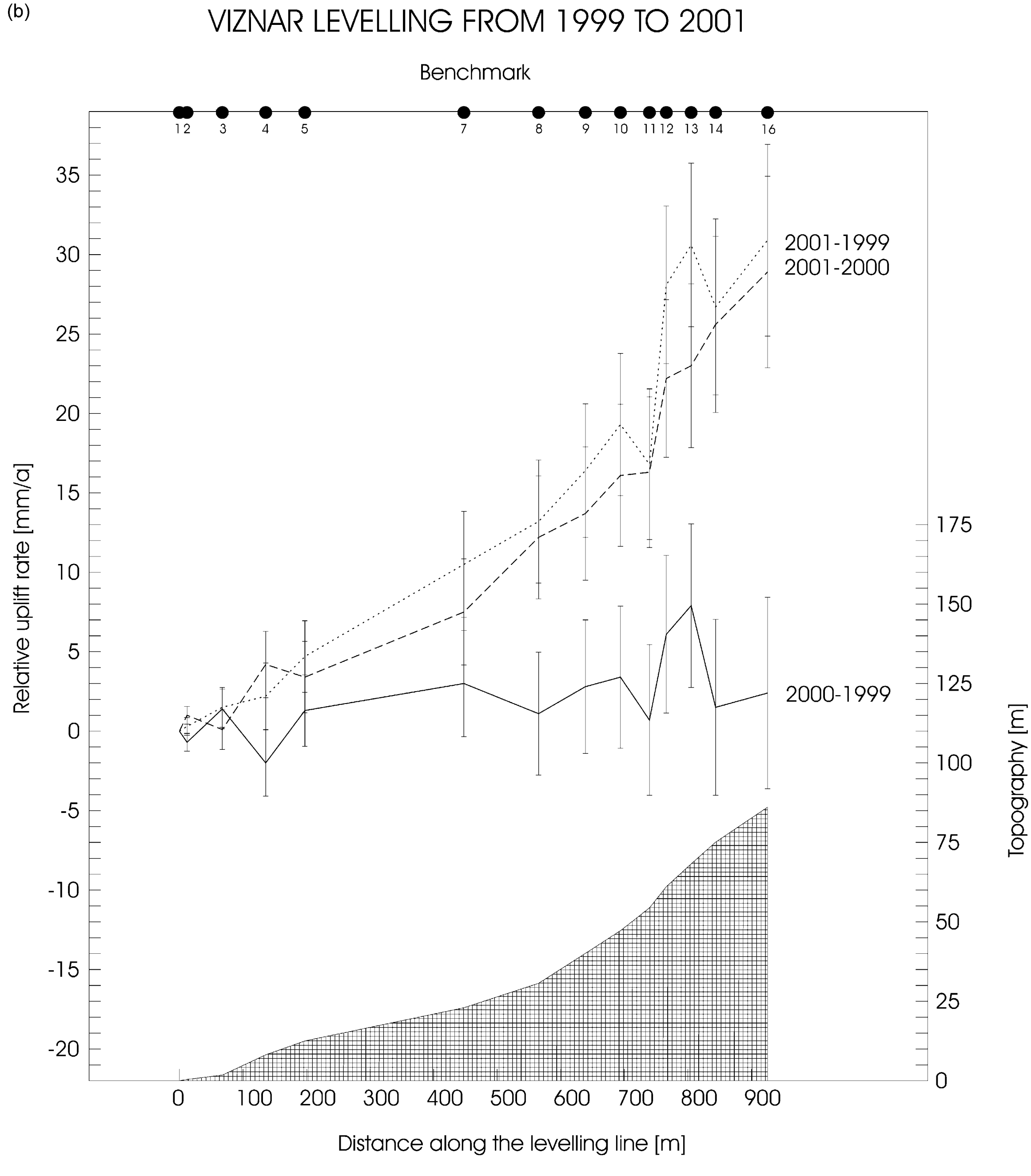

Fig. 6 (*continued*)

where

$$\tan 2\psi = (\dot{\gamma}_1/\dot{\gamma}_2) \tag{8}$$

Both ψ and θ are azimuths measured in degrees clockwise from north. We were able to estimate dilatation parameter as well, but the quality of distance measurements in 1999 is worse than in the rest, so this parameter would not be meaningful and we avoided interpreting it.

In addition, two levelling profiles, each approximately two kilometres long, have been established to measure the level of deformation in the Granada fault. The first (Genil Profile) has fourteen benchmarks and its relief is very smooth (Fig. 6a). The second (Viznar Profile) has sixteen benchmarks and its relief is more pronounced (Fig. 6b).

The height differences between benchmarks of the levelling profiles come from three separate observation campaigns in 1999, 2000 and 2001. The first was surveyed from April to May 1999

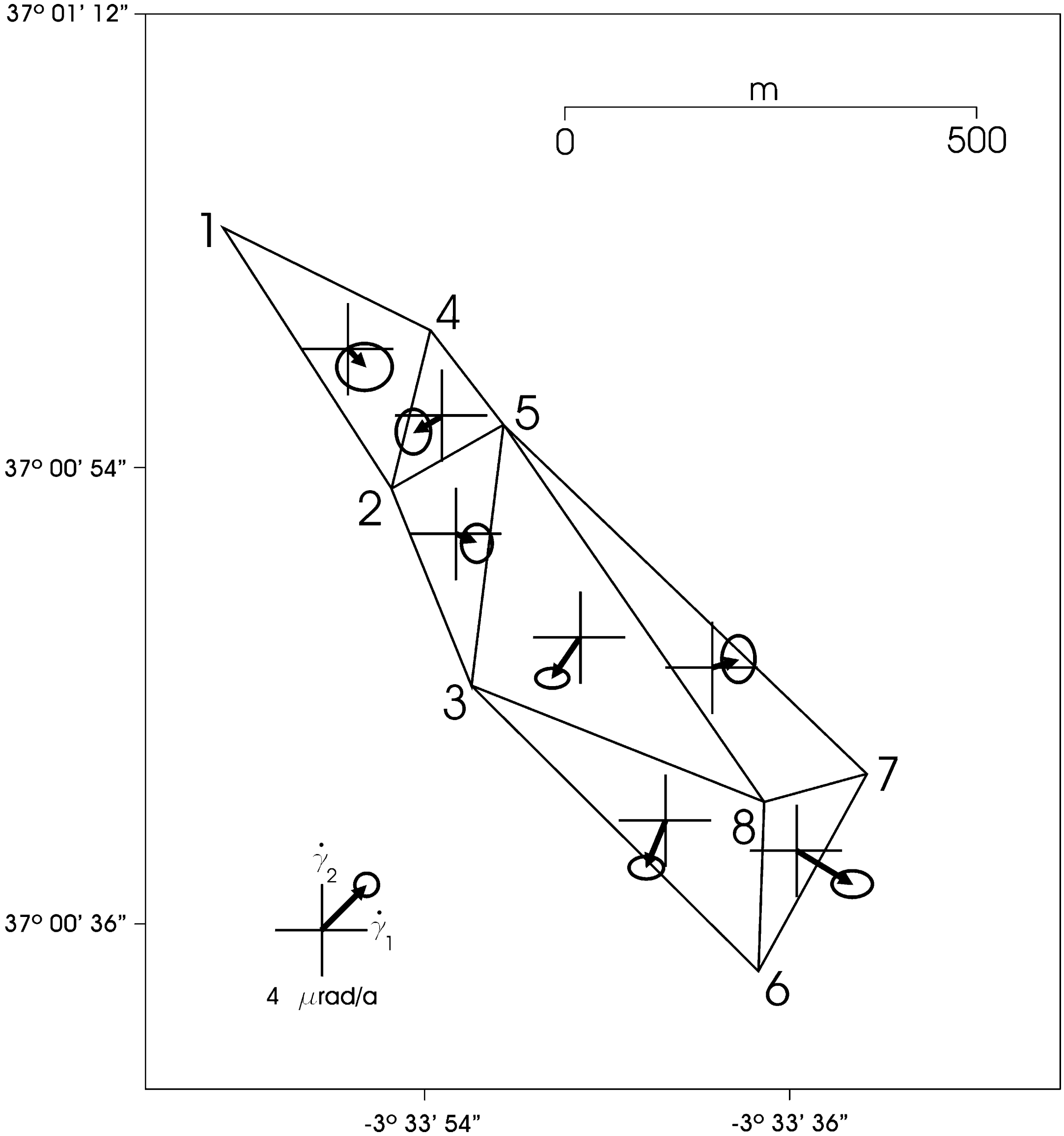

Fig. 7. Shear strain rates (confidence ellipse at 39%) estimated from 1999 to 2001 geodetic inversion at Padul fault geodetic network.

Table 2
Shear strain rates $\dot{\gamma}_1$ and $\dot{\gamma}_2$, total shear rate $\dot{\gamma}$ and the azimuth θ of the axis of the most comprehensive principal strain rate estimated from 1999 to 2001 geodetic inversion

Subnetwork	$\dot{\gamma}_1$ (microradians/a)	$\dot{\gamma}_2$ (microradians/a)	$\dot{\gamma}$ (microradians/a)	θ (°)
1-2-4	1.5±2.5	−1.5±2.1	2.2±2.3	22.7±30.6
2-3-5	1.9±1.4	−0.8±1.6	2.0±1.4	11.9±21.9
2-4-5	−2.5±1.5	−1.5±1.9	2.9±1.6	74.3±18.3
5-7-8	2.3±1.5	0.7±2.0	2.4±1.5	−7.8±23.1
3-5-8	−2.4±1.5	−3.6±0.9	4.3±1.1	61.7±8.9
3-6-8	−1.6±1.5	−4.2±1.0	4.5±1.1	55.3±9.2
6-7-8	4.8±1.7	−3.0±1.2	5.7±1.6	15.9±6.8

The values refer to the subnetworks in Fig. 7. All values show their associated uncertainties.

with a WILD N3 precise level and invar rods, and a WILD NA2000 digital level. The second campaign, February 2000, was performed with two digital levels, a WILD NA2000 and a Leica NA3003. The 2001 campaign has been carried out exclusively with a Leica NA3003 digital level. *Median* mode was used and seven observations were carried out for each measurement to the rod with the NA3003 digital level. When *Median* measurement mode is used with NA3003, small outliers, which appear as systematic collimation falsifications in the very short observation periods of the digital levels, occur much less frequently (Wehmann, 1999). The measuring equipment and field procedures were used according to the rules of precise levelling (Kasser and Becker, 1999). The maximum error in each elevation difference between two benchmarks along the profiles is smaller than 1–2 mm.

4. Results and discussion

At the Padul fault geodetic network, in the planimetric position, displacement vectors are of similar magnitude as propagated errors, so the results show no significant movements in general. Table 2 shows the numerical values of the deformation parameters and their 1σ uncertainties. Strain rate analysis shows that the greatest value of shear strain rate parameters $\dot{\gamma}_1$ and $\dot{\gamma}_2$ are $\dot{\gamma}_1 = 4.8 \pm 1.7$ microradians/a and $\dot{\gamma}_2 = -3.6 \pm 0.9$ microradians/a (Fig. 7; Table 2). These values represent a deformation of 0.5 mm/a in a block zone of 100–200 m, which is the typical size of the subnetwork we used.

As in the planimetric case, the vertical coordinate differences between sites are also in the same magnitude order than the propagated error.

In relation to levelling profiles across the Granada fault, the Genil profile shows small differences between benchmark heights in the three surveys. Height differences between each two consecutive benchmarks at Genil profile comparing all the epochs are less than 1–2 mm. The Viznar profile is more unstable. There are variations between benchmark heights of nearly 1 cm between 2000 and 2001 surveys. Fig. 6a and b shows the vertical relative changes of elevation between the different campaigns with their associated uncertainties. This profile runs along the local Granada-Viznar road, so these movements could be related to ground settlements. In any case, more geodetic data campaigns are needed to correlate the displacements to the local geology and tectonic activity, and to find an appropiate crustal deformation model.

These results agree with geologic evidence and seismicity of the Granada basin, which is located in a low-strain rate environment. There is clearly a need for geodetic determination of crustal strain in the Betic Cordillera, but the low rates, close to the accuracy of the geodetic techniques, and the limitations of the short-timescale observations make such measurement challenging. Further campaigns should provide a longer record of strain accumulation in the region to develop a geodynamic model of faults with a low strain-rate of activity.

Acknowledgements

Reviews by Dr. Giorgio Ranalli and an anonymous referee greatly improved the original manuscript. We are grateful to Leica Geosystems, S.L. company for providing the Leica NA3003 digital level used in the 2000 and 2001 campaigns. We also want to thank Danan Dong for generously sharing his Forward Modelling Network Deformation Analysis Software. This work is supported by the research projects PB97-1267-C03-03 and PB97-1267-C03-01 from the Dirección General de Enseñanza Superior e Investigación Científica.

References

Alfaro, P., Galindo-Zaldívar, J., Jabaloy, A., López-Garrido, A., Sanz de Galdeano, C., 2001. Evidence on the activity and paleoseismicity of the Padul fault (Betic Cordillera, southern Spain). Acta Geológica Hispánica 36, 283–295.

Aguirre, E., 1957. Una prueba paleomastológica de la edad Cuaternaria del conglomerado de la Alhambra. Estudios Geológicos 13, 135–140.

Argus, D.F., Gordon, R.G., DeMets, C., Stein, S., 1989. Closure of the Africa-Euroasia-North America plate motion circuit and tectonics of the Gloria Fault. J. Geophys. Res. 94, 5585–5602.

Bomford, G., 1980. Geodesy. Oxford University Press, Oxford. 855 pp.

Calvache, M.L., Viseras, C., Fernández, J., 1997. Controls on fan development-evidence from fan morphometry and sedimentology; Sierra Nevada, SE Spain. Geomorphology 21, 69–84.

De Miguel, F., Vidal, F., Alguacil, G., Guirao, J.M., 1989. Spatial and energetic trends of the microearthquakes activity in the Central Betics. Geodin. Acta 3, 87–94.

DeMets, C., Gordon, G., Argus, D.F., Stein, S., 1994. Effect of recent revisions to the geomagnetic reversal time scale on estimate of current plate motions. Geophys. Res. Lett. 21 (20), 2191–2194.

Dong, D., 1993. The Horizontal Velocity Field in the Southern California from a Combination of Terrestrial and Space-Geodetic Data. PhD. thesis, Mass. Inst. of Technol., Cambridge, 157 pp.

Dong, D., Herring, T.A., King, R.W., 1998. Estimating regional deformation from a combination of space and terrestrial geodetic data. J. Geod. 72 (4), 200–214.

Estévez, A., Sanz de Galdeano, C., 1983. Néotectonique du secteur central des Chaînes Bétiques (Basins du Guadix-Baza et de Grenade). Revue de Géographie Physique et de Géologie Dynamique 21, 23–34.

Feigl, K.L., King, R.W., Jordan, T.H., 1990. Geodetic measurement of tectonic deformation in the Santa Maria Fold and Thrust Belt, California. J. Geophys. Res. 95 (B3), 2679–2699.

Ferhat, G., Feigl, K.L., Ritz, J.F., Souriau, A., 1998. Geodetic measurement of tectonic deformation in the southern Alps and Provence, France, 1947–1994. Earth Planet. Sci. Lett. 159, 35–46.

Galindo-Zaldívar, J., Jabaloy, A., Serrano, I., Morales, J., González-Lodeiro, F., Torcal, F., 1999. Recent and present-day stresses in the Granada Basin (Betic Cordilleras): example of a late Miocene-present-day extensional basin in a convergence plate boundary. Tectonics 18 (4), 686–702.

Gil, A.J., Ruiz, A.M., Borque, M.J., Rodríguez-Caderot, G., de Lacy, M.C., Sanz de Galdeano, C., Alfaro, P., Ruiz, M., Crespi, M., Biagi, L., 1999. Ground Deformation Monitoring in the Central Sector of Betic Cordillera (Spain) from Geodetic Techniques: Status Report. Poster of the International Union of Geodesy and Geophysics. Birmingham, UK, July 1999.

Gil, A.J., Ruiz, A.M., Rodríguez-Caderot, G., de Lacy, M.C., 2000. Deformation Studies in Padul-Nigüelas and Granada City Faults. Poster of the European Geophysical Society. XXV General Assembly. Nice, France, April 2000.

Herraiz, M., De Vicente, G., Lindo-Ñaupari, R., Giner, J., Simón, J.L., González-Casado, J.M., Vadillo, O., Rodríguez-Pascua, M.A., Cicuéndez, J.I., Casas, A., Cabañas, L., Rincón, P., Cortés, A.L., Ramírez, M., Lucini, M., 2000. The recent (upper Miocene to Quaternary) and present tectonic stress distributions in the Iberian Peninsula. Tectonics 19 (4), 762–786.

Kasser, M., Becker, J.M., 1999. Error sources in high precise levelling. In: Proceedings of Geodesy and Surveying in the future. The importance of Heights. FIG commission 5, Gävle, Sweden, March 1999, pp. 213–222.

Keller, E.A., Sanz de Galdeano, C., Chacón, J., 1996. Tectonic geomorphology and earthquake hazard of Sierra Nevada, South Spain. In: Proceedings of the 1 Conferencia Internacional Sierra Nevada, Granada, Spain, March 1996, pp. 201–218.

Laurila, S.H., 1983. Electronic Surveying in Practice. John Wiley & Sons Inc, New York. 388 pp.

Lhénaff, R., 1965. Néotectonique quaternaire sur le bord occidental de la Sierra Nevada (province de Grenade, Espagne). Revue de Géographie Physique et de Géologie Dynamique (2) 205–207.

Prescott, W.H., Savage, J.C., Kinoshita, W.T., 1979. Strain accumulation in the western United States between 1970 and 1978. J. Geophys. Res. 84 (B10), 5423–5435.

Riley, C., Moore, J.McM, 1993. Digital elevation modelling in a study of the neotectonic geomorphology of the Sierra Nevada, southern Spain. Z. Geomorph. N. F 94, 25–39.

Ruiz, A.M., Gil, A.J., Rodríguez-Caderot, G., de Lacy, M.C., 1999. Local geodetic control to detect ground movements in Betic Cordillera (Spain). In: Proceedings of The 9th FIG International Symposium on Deformation Measurements. Olsztyn (Poland), September 1999, pp. 64–70.

Ruiz-Bustos, A., 1972. Mamíferos del Pleistoceno Inferior de la Provincia de Granada. Tesis de Licenciatura. University of Granada. Spain.

Ruiz-Bustos, A., Fernández, J., Morales, J., Rodríguez-Fernández, J., Vera, J.A., 1990. Los materiales Plio-Pleistocenos del borde norte de la Depresión de Granada. Estudios Geológicos 46 (3/4), 277–290.

Santanach, P., Sanz de Galdeano, C., 1980. Bousquet, Neotectónica de las regiones mediterráneas de España. Bol. Inst. Geol. Min. 91-92, 417–440.

Sanz de Galdeano, C., Peláez, J.A., López-Casado, C. Seismic potentiality of the main active faults in the Granada Basin (South of Spain). Pure and Applied Geophysics (in press).

Sanz de Galdeano, C., López Garrido, A.C., 1999. Nature and impact of the Neotectonic deformation in the western Sierra Nevada (Spain). Geomorphology 30, 259–272.

Sanz de Galdeano, C., 1996. Neotectónica y tectónica activa en el sector Padul-Dúrcal (Borde SW de Sierra Nevada, España). In: Proceedings of the 1ª Conferencia Internacional Sierra Nevada, Granada, March, 1996, pp. 219–231.

Savage, J.C., Prescott, W.H., 1973. Precision of geodolite distance measurements for determining fault movements. J. Geophys. Res. 78 (26), 6001–6008.

Wehmann, W., 1999. Experience with various digital levels in both motorised and conventional "on foot" precise levelling in east Germany. In: Proceedings of Geodesy and Surveying in the future. The importance of Heights. FIG commission 5, Gävle, Sweden, March 1999, pp. 95–106.